Sedimentary Geology 235 (2011) 27–37

Contents lists available at ScienceDirect

Sedimentary Geology

journal homepage: www.elsevier.com/locate/sedgeo

Cretaceous oceanic red beds as possible consequence of oceanic anoxic events

Chengshan Wang [a,*], Xiumian Hu [b,*], Yongjian Huang [a], Michael Wagreich [c], Robert Scott [d], William Hay [e]

[a] State Key Laboratory of Geological Processes and Mineral Resources, China University of Geosciences, Beijing 100083, China
[b] Department of Earth Sciences, Nanjing University, Nanjing 210093, China
[c] Department of Geodynamics and Sedimentology, University of Vienna, A-1090 Vienna, Austria
[d] University of Tulsa, 149 West Ridge Road, Cleveland, OK 74020, USA
[e] Department of Geological Sciences, University of Colorado at Boulder, 399 UCB, Boulder, CO 80309-0399, USA

ARTICLE INFO

Article history:
Received 13 July 2009
Received in revised form 10 June 2010
Accepted 25 June 2010
Available online 7 July 2010

Keywords:
Cretaceous
Black shales
Oceanic red beds
Oceanic anoxic events
Paleoceanography
Paleoclimate

ABSTRACT

Oceanic Anoxic Events (OAEs) represent brief periods of burial of large amounts of organic carbon in the oceans during Cretaceous time. Burial of organic carbon, which preferentially sequestered isotopically lighter carbon during OAEs, resulted in positive $\delta^{13}C$ excursions of 2–3‰ recognizable in global ocean. These deposits are typically dark–grey to black shales, considered to be the result of interaction between extreme warm climate, ocean circulation, high bioproductivity and organic carbon preservation. Less interest has been given to periods between OAEs, when oxic deep sea deposits such as red marls and red shales were deposited during mid- and Late Cretaceous. The latter deposits are associated with very low content of organic carbon and oxic depositional environments which dominated western Tethys in post Turonian time, up to the early Eocene.

Feedbacks among geochemical cycles in response to decreasing global temperatures, increasing deep ocean circulation forced by high-latitude deep water formation along the Antarctic margin, and widening and deepening of the interconnections between the oceanic basins may have been responsible for the major paleoceanographic change from deposition of organic carbon-rich black shales during mid-Cretaceous, to world-wide deposition of Cretaceous Oceanic Red Beds (CORBs) in the Late Cretaceous. The presence of CORBs sandwiched between mid-Cretaceous OAEs may reflect major climate and paleoceanographic changes. In a contrast to extremely warm climates during the OAEs, the CORBs suggest cold periods, and therefore oscillating climate shifts, that have seldom been considered during modeling of Cretaceous greenhouse climate and global carbon cycling.

1. Introduction

Earth's climate has oscillated between greenhouse (warm) and icehouse (cold) modes during the Phanerozoic. At present, Earth is in the midst of an icehouse climate, despite the rise of industrialization during past two centuries, which has led to dramatic increase in atmospheric CO_2 from burning of fossils fuels. This, in turn, has led to significant global warming (e.g. Ruddiman, 2001). Global warming could profoundly impact human civilization by major env\ironmental changes, such as sea-level rise resulting in coastal flooding, changes in precipitation, desertification, increased storm and hurricane frequency and changes of El Niño. Thus understanding of the ocean-climate system during past greenhouse climate modes is essential for more accurate prediction of future climate and environmental changes on a warming earth. One such period of a typical greenhouse, caused largely by increases in CO_2 from elevated global igneous activity, is the Cretaceous–early Cenozoic era.

The mid-Cretaceous is marked by a major warming peak, characterized by globally averaged surface temperatures more than 14 °C higher than those of today (Tarduno et al., 1998), absence of permanent ice sheets (Frakes et al., 1992), and sea level 100–200 m higher than that of today (Haq et al., 1987). Atmospheric carbon dioxide levels are thought to have been 4 to 10 times higher than those of the pre-industrial era (Berner and Kothavala, 2001; Bice and Norris, 2002; Huber et al., 2002).

Black shales containing 2–30% organic carbon were episodically deposited in oceanic and marginal basins during Cretaceous time and are commonly referred to as "oceanic anoxic events" (OAEs) (Leckie et al., 2002; Erba, 2004). The conditions of their deposition have been intensively debated as to the relative importance of high marine productivity versus oceanic water stratification and stagnation. Even though the concept of OAEs as a global phenomenon was put forward 30 years ago (Schlanger and Jenkyns, 1976), it still remains a topic of intensive research due to the significance of burial of large amount of

* Corresponding authors. Wang is to be contacted at Tel.: +86 10 8232 1612; fax: +86 10 8232 2171. Hu, Tel.: +86 25 8359 3002; fax: +86 25 8368 6012.
E-mail addresses: chshwang@cugb.edu.cn (C. Wang), huxm@nju.edu.cn (X. Hu), huangyj@cugb.edu.cn (Y. Huang), michael.wagreich@univie.ac.at (M. Wagreich), rwscott@ix.netcom.com (R. Scott), whay@gmx.de (W. Hay).

0037-0738/$ – see front matter.
doi:10.1016/j.sedgeo.2010.06.025

organic matter in deep-sea sediments and of carbon cycling and its effect on global climate. Eight intervals of the OAEs are recorded by Cretaceous oceanic sediments, but only two of them — the OAE1a (~122 Ma, with duration ~800 ky) and OAE2 (~93.5 Ma with duration 300 ky) have well documented global distribution (Leckie et al., 2002; Erba, 2004).

Later in the Cretaceous, the climate cooled as carbon dioxide levels in the atmosphere declined (Clarke and Jenkyns, 1999). The largest drop in global temperature occurred in the early Campanian, marking the transition from a "hot" to "cool" greenhouse climate (Clarke and Jenkyns, 1999; Huber et al., 2002). Possible causes of the decrease in atmospheric CO_2 leading to global cooling are the reduction in seafloor volcanic activity (Larson, 1991) and burial of large amounts of organic carbon (Berner, 2003). The latest Cenomanian Anoxic Event (OAE2) resulted in burial of 1.6×10^{18} moles of organic carbon within 0.5 m.y., causing significant depletion of CO_2 in the ocean-atmospheric system (Arthur et al., 1988; Kuypers et al., 1999). Post OAE2 depositional conditions in the Tethys ocean changed dramatically, as deposition of black shales was replaced by deposition of pelagic red beds (CORBs). The latter are widely distributed Cretaceous oceanic deposits, as shown by compilation of locations of CORBs (Figs. 1B and 2B) (Wang et al., 2009), which lasted longer than the OAEs (Figs.1A and 2A) (Scott, 2009). However, earlier episodes of major climate change are

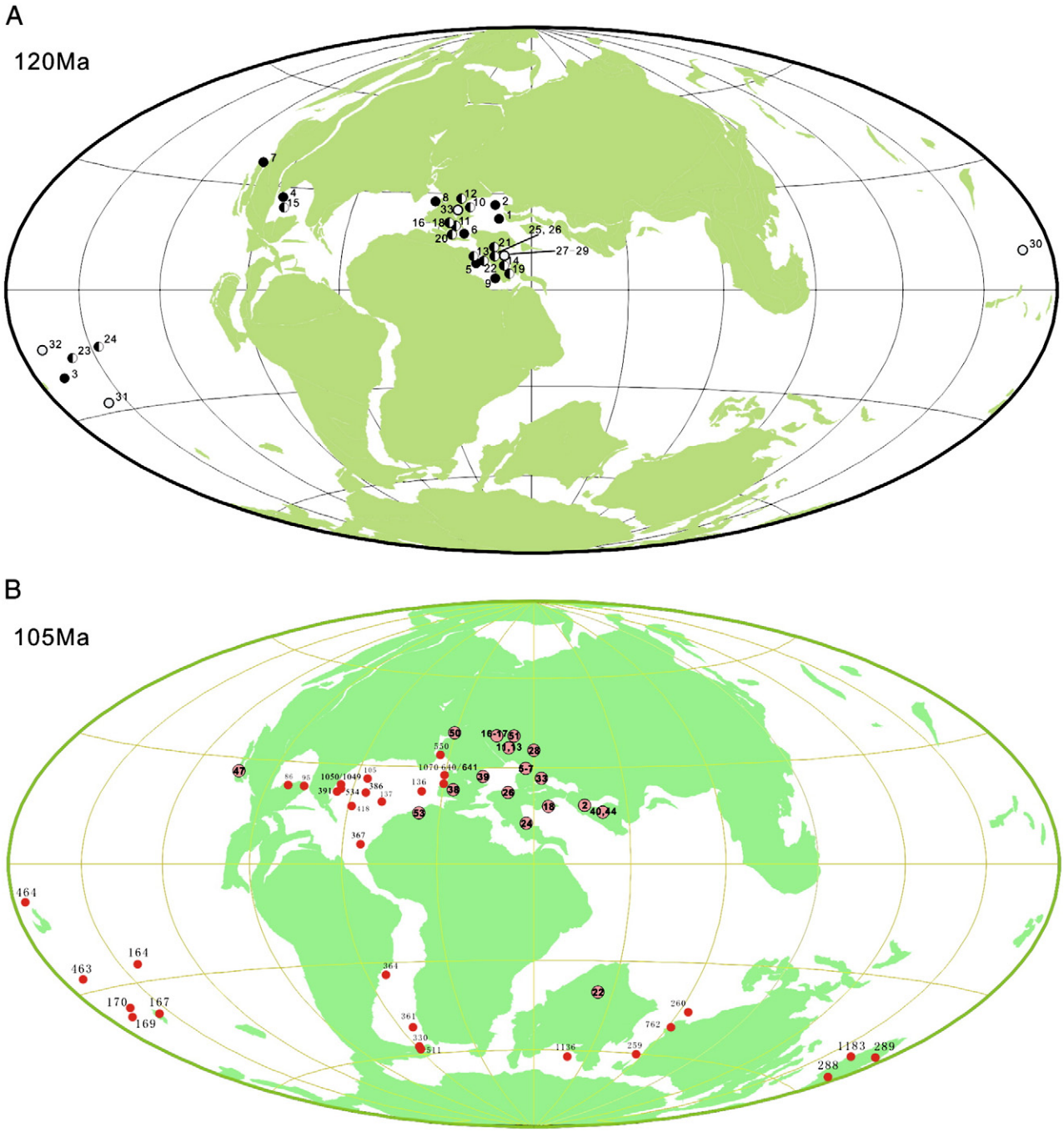

Fig. 1. Paleogeographic map showing the occurrence of OAE1a and CORBs at 120 Ma and 105 Ma. A) Distribution of OAE1a, early Aptian (120 Ma) data from published literature (Appendix 1), keys for the symbols: ● – all three characteristics features of black shales, a high content of OM and excursions of $\delta^{13}C$; ◐ – two of the three characteristics features; ○ – one of the three characteristics features; B) Distribution of CORBs at 105 Ma cited from Wang et al. (2009). The paleogeographic base map was downloaded from the website www.odsn.de.

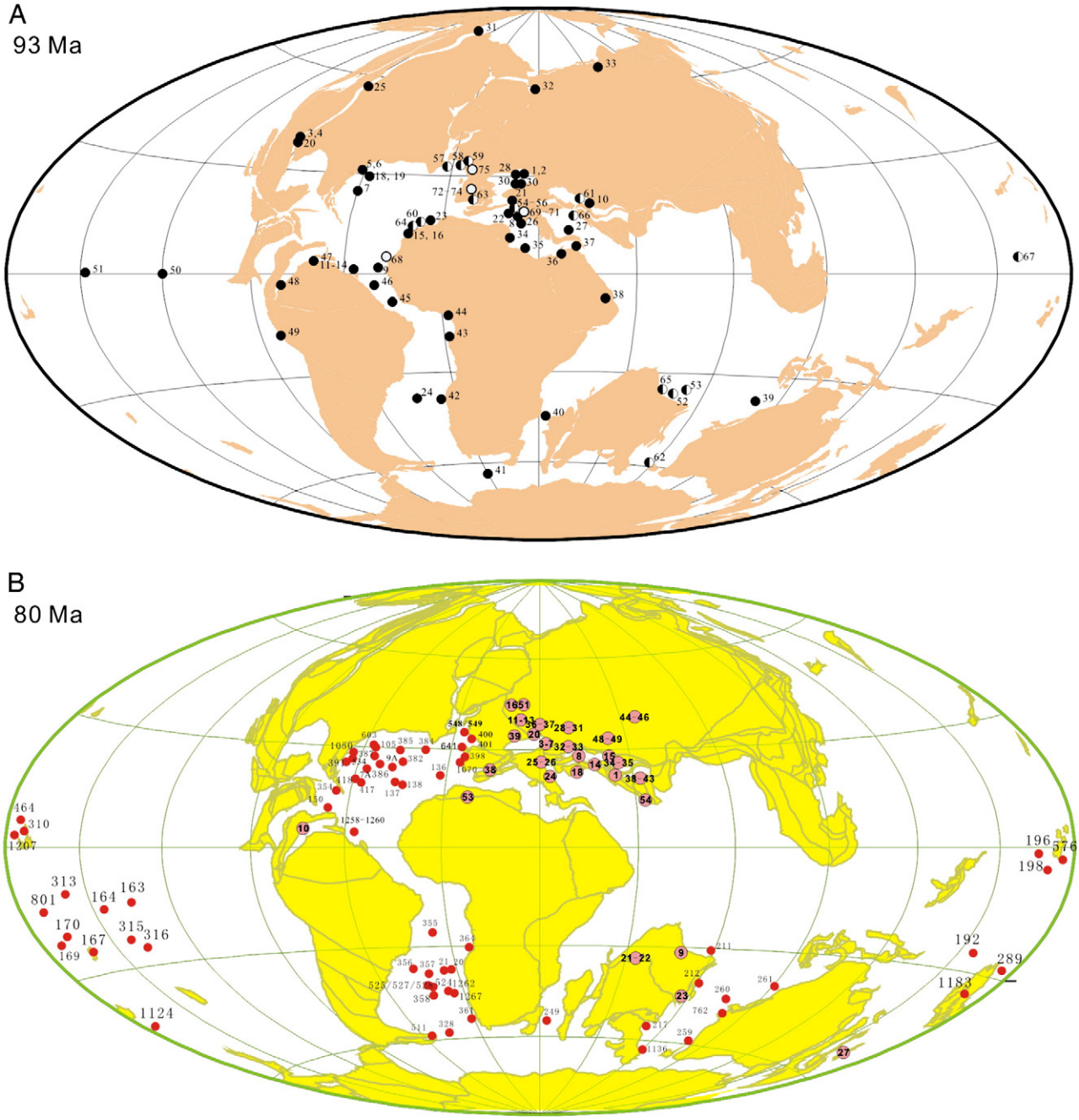

Fig. 2. Paleogeographic map showing the localities and the correlation of OAE2 and CORBs in 80 Ma. A) Distribution of OAE2, Cenomanian–Turonian (93 Ma) data from published literature (Appendix 1) keys for the symbols: ● – all three characteristics features of black shales, a high content of OM and excursions of $\delta^{13}C$; ◐ – two of the three characteristics features; ○ – one of the three characteristics features. B) Distribution of CORBs at 80 Ma cited from Wang et al. (2009). The paleogeographic base maps are downloaded from the website www.odsn.de.

evidenced by episodic deposition of CORBs sandwiched between OAEs in the mid-Cretaceous (Hu et al., 2006a). Such changes document much more variable climatic conditions during the mid-Cretaceous and a higher complexity of the ocean-climate-carbon burial system than presented by system modeling.

Here we report on the distribution of CORBs in the Upper Cretaceous sedimentary sequences of the oceanic basins, and explore their relationship to the global paleoclimatic and paleoceanographic changes that occurred during the Late Cretaceous. The aim is to investigate the hypothesis that there was a causal relationship between OAEs and CORBs and, if so, what the major drivers of such change might have been. Future research will be oriented toward correlating oceanic OAEs and CORBs with continental sequences, to determine the climatic consequences of these events on land.

2. Temporal–spatial distribution of Cretaceous OAEs and CORBs

In order to compare the temporal and spatial relation between the OAEs and the CORBs, we made a new compilation of their occurrence and distribution. Since the OAEs have been studied for more than 30 years, the compilation relies mainly on published literature (Appendix 1). OAEs occurred at least eight times during the Cretaceous. The OAE1a and OAE2 represent global-scale anoxic events associated with prominent positive excursions of $\delta^{13}C$ and worldwide

distribution of black shales. Data collected for the black shales of OAE1a and OAE2 have focused on three features: lithofacies, high content of organic matter (OM) and positive excursions of $\delta^{13}C$ (Arthur and Sageman, 1994) which are useful markers for OAE recognition (e.g., Takashima et al., 2004).

The compilation utilized here for CORBs is based on a review paper (Wang et al., 2009). To better show CORBs distribution, we plotted the locations of oceanic red beds on two time slice paleogeographic maps (Figs. 1B and 2B). The CORBs of mid-Cretaceous (Aptian–Cenomanian) were shown on the paleogeographic map of 105 Ma (Fig. 1B), while the CORBs of Late Cretaceous (Turonian–Maastrichtian) were shown on the paleogeographic map of 80 Ma (Fig. 2B). The CORBs became increasingly widespread from the Aptian through the Campanian, attaining global distribution during the Late Santonian and Early Campanian (Figs. 1B and 2B) and continuing in western Tethys up to the Early Eocene. CORBs were preferentially deposited in the middle to low latitude basins of the Tethys, Atlantic, Indian, and Panthalassic (Pacific) Oceans. Outcrops of these red beds have been found in the Tibetan Tethyan Himalaya, Caucasus, Turkey, Carpathians, and Alps and southern Europe (Spain, Italy). Localized high latitude deposits are found in New Zealand and in the South Atlantic (Figs. 1B and 2B). The depositional environments include outer-shelf, continental slope, and deep sea. Because of local tectonics, CORBs are exposed widely in the western Tethys, but are preserved only as remnants in the orogenes of the eastern Tethys. They have also been recovered from ODP/DSDP Legs in the abyssal plains of the Atlantic and Pacific Oceans. CORBs closely overlie OAE black shales at many locations (see below).

The distribution of OAE1a and subsequent mid-Cretaceous CORBs are shown on the paleogeographic reconstructions for 120 Ma and 105 Ma, respectively. They are found mainly in the Western Tethys, Pacific Ocean, Gulf of Mexico, and Atlantic Ocean (Fig. 1A), with the western Tethys being the most studied region. Many mid-Cretaceous CORBs occur in the Eastern Tethys and Indian Ocean, but no record of OAE1a was found in these areas.

OAE2 and subsequent Late Cretaceous CORBs, plotted on 93 Ma and 80 Ma paleogeographic maps, respectively, show co-occurrence in Western Tethys, Atlantic Ocean, Eastern Tethys, Pacific Ocean, and Indian Ocean (Fig. 2A). The Western Interior Seaway and Arctic Ocean are distinctive by recording the occurrence of OAE2 lacking associated CORBs. On the other hand, CORBs are more commonly recorded in deep oceanic sediments than deposits of OAE2.

3. Transition from oceanic anoxic events to red beds in Tethys

To better understand the relationship between the OAEs and CORBs, we have studied two stratigraphic intervals in the Tethys realm in detail: from OAE1a to Aptian oceanic red beds (ORB1; Hu et al., 2006), and from OAE2 to Turonian oceanic red beds (ORB9; Hu et al., 2009).

3.1. OAE1a–ORB1 transition

3.1.1. Gorgo a Cerbara section, Italy

The Gorgo a Cerbara section is located 3 km west of the town of Piobbico (Marche, Italy). OAE1a (the Selli Level) (Figs. 3A and 4) is 1.92 m thick and consists of laminated to bioturbated olive-grey, greenish-grey and dark-grey to black mudstones and shales, with 20 thin (1 to 3 cm) greyish-yellow, olive-grey and medium- to dark-grey radiolarian silty/sandy layers (Coccioni et al., 1987, 1989, 1992). TOC contents of 16 samples from the Selli Level from the Gorgo a Cerbara section ranged from 0.74–7.28% (Baudin et al., 1998). A 2.5 m thick stratigraphic interval separates the Selli Level and ORB1 (Figs. 3A and 4). It is lithologically characterized by bioturbated greenish-grey cherty limestones, marly limestones with subordinate marls, in beds 1- to 30-cm thick. ORB1 is over 15 m thick at the Gorge a Cerbara section. It is dominated by bioturbated, dark red marlstone, red marly limestones

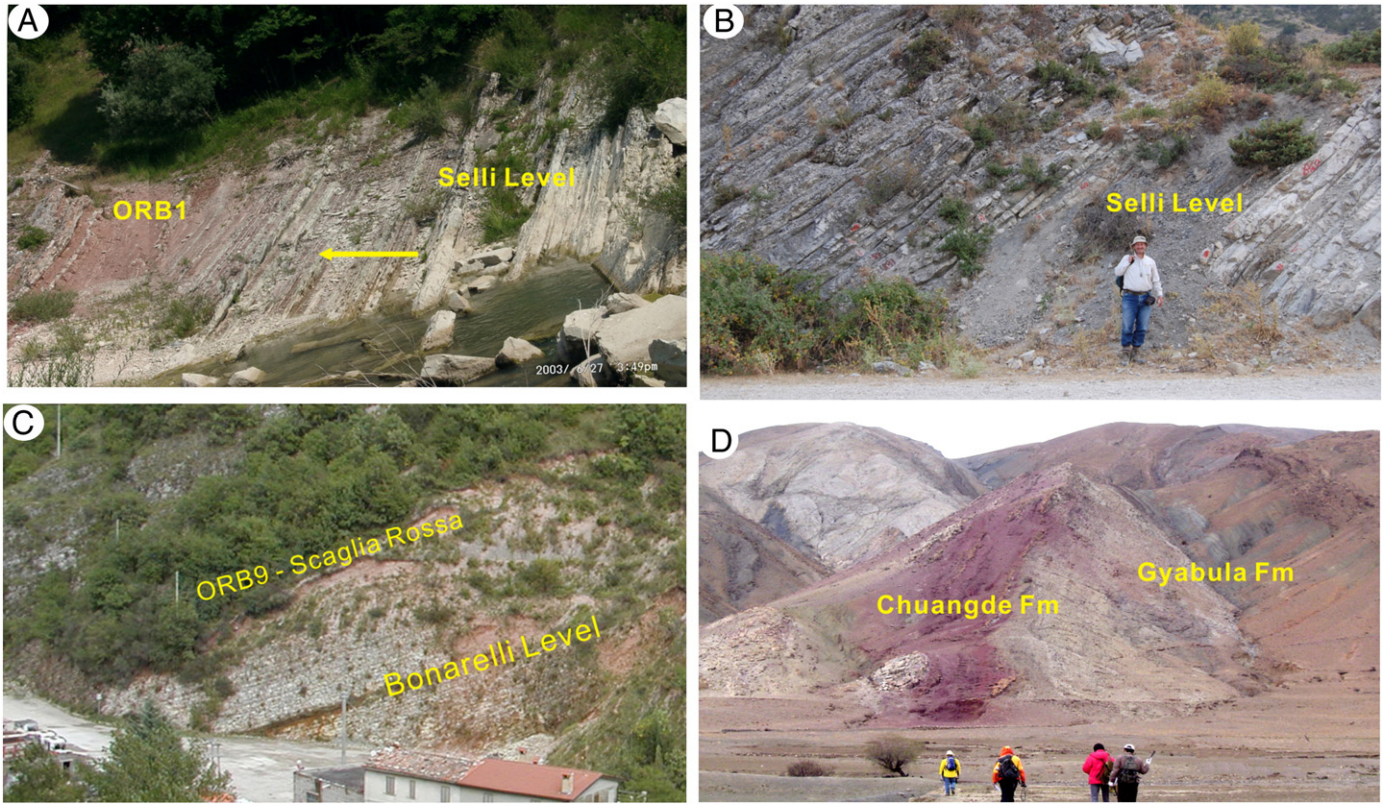

Fig. 3. Photos showing the sections studied. A – Gorgo a Cerbara section, central Italy; B – Mudurnu section, central Turkey; C – Vispi Quarry section, central Italy; D – Chuangde section, south Tibet.

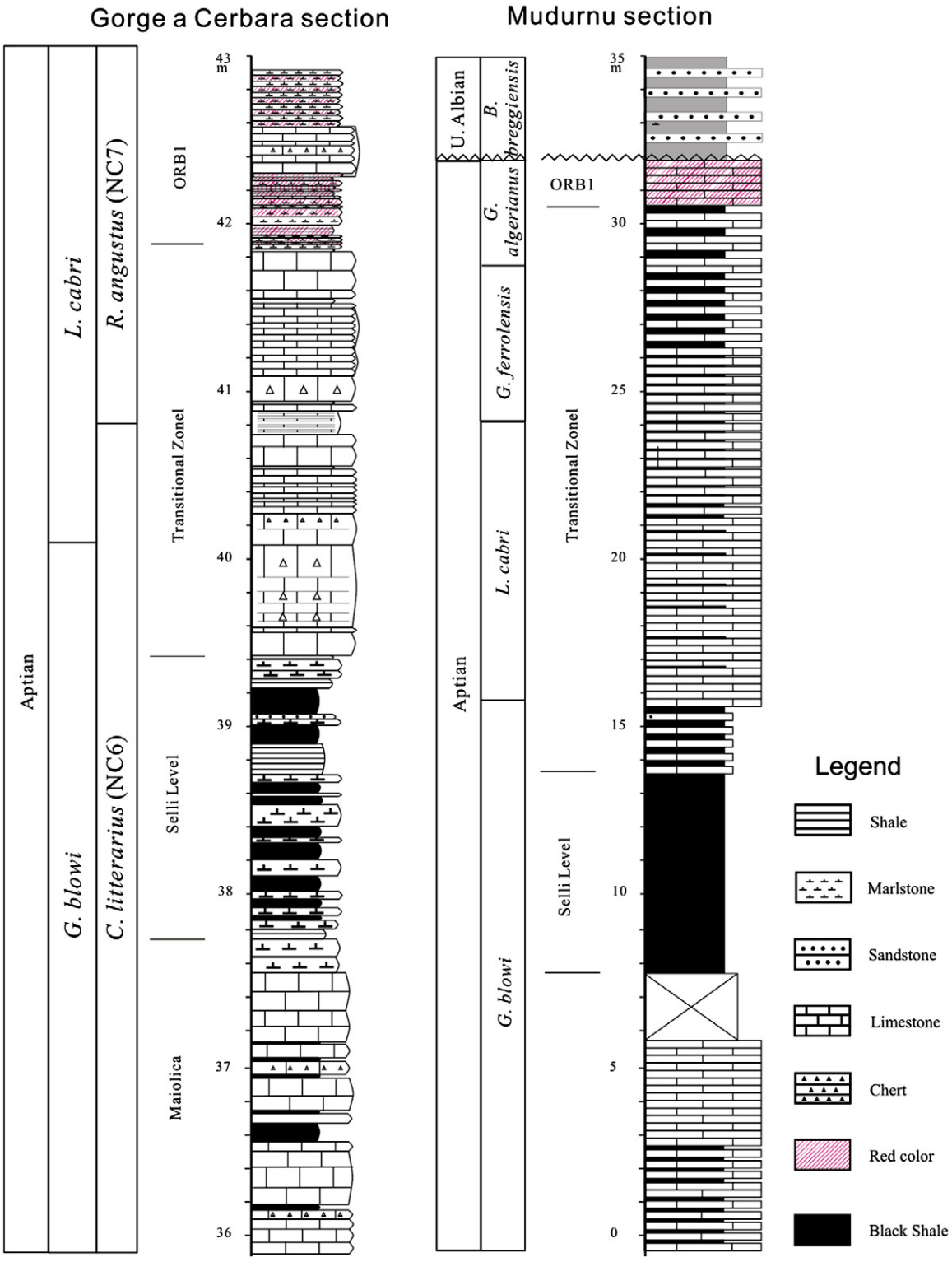

Fig. 4. Stratigraphic log of the OAE1a–ORB1 transition in the Gorgo a Cerbara and Mudurnu sections (revised from Yilmaz, 2008).

and red calcareous shales with subordinate gray marlstones and marly limestones, in beds 1- to 30-cm-thick. The gray beds are locally interbedded with red beds in a cyclical manner. The red beds are generally less calcareous than the gray beds. The contacts between red beds and gray beds are commonly sharp. Within the intercalated gray beds, the color becomes more reddish in zones a few mm-thick, both near the base and the top of the beds. If we apply the 2.6 m/myr sedimentation rate for the interval from the base of M0 (35.6 m) to the top of the *C. litterarius* zone (40.8 m) of Coccioni et al. (1992), it took about 0.95 myr for the change from the top of the Selli Level to the deposition of first reddish limestone of the ORB1 (Hu et al., 2006a).

3.1.2. Piobbico core, Italy

In the Piobbico core, the Selli Level is located in Unit 18, which is about 2.36 m thick (73.47 m–75.83 m level of Erba, 1988). It is composed of black shale in beds 1- to 15-cm-thick, with abundant

pyrite nodules, radiolaria and fish remains. Overlying the Selli Level is a zone about 3 m thick which consists of gray-green marly limestones and limy marls in beds 2–20 cm thick. ORB1 in Piobbico Core corresponds to Units 15 and 17 (53.14 m–70.65 m level of Erba, 1988) and is represented by dark-red and dark-brown marls and marly limestones with few green-gray colored calcareous marls and marly limestones. Black shales are absent throughout the ORB1 interval. If we apply the 2.3 m/myr sedimentation rate of the *L. cabri–G. algerianus* zones of Tornaghi et al. (1989), it took about 1.2 myr for the change from the top of the Selli Level to the first reddish limestones of ORB1 (Hu et al., 2006a).

3.1.3. Mudurnu, Turkey

In NW Turkey the Selli Level is about 2.2 m thick at Mudurnu (Yilmaz, 2008) (Figs. 3B and 4). The black shales of the Selli Level display cm-to m-scale cycles, shales with pyritized radiolaria, and planktonic foraminifera with iron-coated chambers. The ORB1 is about 2 m thick and was assigned to the *G. algerianus–P. cheniourensis* zones. It consists of red to pink limestones (mainly packstones) and marls. The ORB1 is cut by "Neptunian dyke"-like features disconformable with the overlying Upper Albian turbiditic strata (Yilmaz, 2008). A stratigraphic zone between the Selli Level and CORB2 is about 22 m thick and consists of whitish marly limestones interbedded with calcareous marls and/or shales. Some calcareous turbiditic beds up to few cm thick occur within this transitional zone. If we assume an approximately 7.5 m/myr sedimentation rate for this strata, it took about 2.9 myr for the change from the top of the Selli Level to the first reddish limestones of the ORB1 at the Mudurnu locality (Yilmaz, 2008).

3.2. OAE2–ORB9 transition

3.2.1. Vispi Quarry, Italy

In the Vispi Quarry near Gubbio, Italy, above the Bonarelli bed 4.3 m of white limestones limestone of the Scaglia Bianca grade into a sequence of predominantly pinkish–reddish limestones and marls of the Scaglia Rossa Formation (Hu et al., 2006a and references within) (Figs. 3C and 5). Below the reddish limestone successions are two transitional beds (the lower at 10.35–10.55 m and the higher at 10.63–10.83 m). Both transitional beds are whitish in color at the base and gradually become increasing pinkish in color towards the top. The strata above 10.83 m are pinkish to reddish. If we apply the 7.4 m/myr sedimentation rate of the *H. helvetica* zone of Premoli Silva and Sliter (1994), it took about 1.5 myr for the change from the top of the Bonarelli Level to the predominantly red colored limestones of the Scaglia Rossa Formation (ORB9) (Hu et al., 2006a).

3.2.2. Buchberg section, Austria

The Buchberg section, Austria, exposes a Cenomanian–Turonian succession of limestones, marly limestones and marlstones with Cenomanian strata being not fully exposed (Fig. 5) (Neuhuber et al., 2007; Wagreich et al., 2009). Light grey limestones with dark grey mottles alternate with medium and dark grey spotty marlstones at the base of the section. They are overlain by grey and red limestones and marlstones of Turonian age; pink marl is 2 to 3 m above beds of OAE2 and red limestone is 5 m above (Wagreich et al., 2009, Fig. 6). This interval represents a duration of approximately 1.1–1.5 Myr (Neuhuber et al., 2007; Scott, 2009). At the top of the section the Ultrahelvetic rocks are overthrusted by sandstone debris of the Rhenodanubian Flysch Zone. The Ultrahelvetic section consists of alternating limestone–marl cycles with four transitions of grey-colored intervals into red beds. In the lower part of the profile, the red color is restricted to marl beds whereas in the upper part of the section both marl and limestone beds are red (Wendler et al., 2009). The bedding planes are even to wavy planes and the beds tend to be more bioturbated at the top of the profile. The sediment accumulation rate of the red beds was about 3 m/myr (Scott, 2009).

3.2.3. Chuangde section, Tibet

At the Chuangde locality (Fig. 3D) in southern Tibet, the 30-meter-thick Chuangde Formation consists of reddish-colored mudstone intercalated with pelagic marlstone, limestone, and radiolarian chert. The strata were deposited in a slope-basin environment (Wang et al., 2005). They conformably overlie the black shales of the Gyabula Formation, interpreted as corresponding to mid-Cretaceous OAEs (Wang et al., 2001; Wan et al., 2003). The red beds contain abundant planktonic foraminifera dated as Late Santonian to Early Campanian (Wan et al., 2005). The sediment accumulation rate of the red beds was about 2.66 m/myr (Scott, 2009), which is higher than that of modern un-compacted oceanic red clays (Glasby, 1991). Deposition of the Chuangde CORB began approximately 9 myr after the OAE2 event and about 1 myr after OAE3, which is not recorded in this Tibet section (Scott, 2009). To test the hypothesis a section where the Chuangde overlies a complete Santonian interval is needed.

4. Paleoceanographic response to the OAE2–ORB9 transition: a case study from Chuangde section, Tibet

Due to its characteristic reddish color, the Chuangde Formation is a marker unit in the Gyangze area (Wang et al., 2005). It consists of reddish-colored mudstone intercalated with pelagic marlstone, limestone, and radiolarian chert; its basal and upper contacts are distinct and sharp. The color of the red beds, no matter what is the lithology, is uniformly red. This is not the result of modern weathering, but is a depositional feature. Unlike terrigenous red beds, there are no oxidized ferric rims on the particle margins. X-Ray diffraction demonstrates that the red coloration is the result of minute non-crystalline hematite particles dispersed throughout the red beds (Hu et al., 2006b), as is similarly the case in coeval CORBs from Italy and Turkey (Channel et al., 1982; Eren and Kadir, 2001). The $Fe^3/(Fe^{2+}+Fe^{3+})$ ratio ranges from 0.51 in the black shale to 0.99 in the red unit with a maximum Fe_2O_3 level as high as 10% in the red shales (Wang et al., 2005).

The ratio between the reactive iron species (Fecarb: carbonate-associated iron; Feox: ferric iron oxides-goethite and hematite; Femag: magnetite; Fepy: pyrite; FeHR: the sum of the four iron species) and total iron (FeT) can reflect the change of iron species in different depositional environments (Lyons and Severman, 2006). Those five ratios were determined by using a sequential chemical extraction method (Poulton and Canfield, 2005) on samples from Gyabula and Chuangde formations.

The average of Feox/FeT, Femag/FeT, FeHR/FeT ratios are 0.296, 0.067, 0.37, respectively, in the red beds of Chuangde Formation, which contrast with mean ratios of 0.10, 0.028 and 0.l61 in the black shales of Gyabula Formation (Fig. 6). Fecarb/FeT and Fepy/FeT ratios in the black shales are 0.031 and 0.0015, much higher than that of red beds (0.006 and 0 on average). Most of the iron in different reactive iron species in marine sediments is ultimately derived from continental iron oxides (Raiswell and Canfield, 1998). Assuming that weathering conditions in the source area have not changed greatly during the Cretaceous (Hu et al., 2006b), the much lower Feox/FeT, Femag/FeT, FeHR/FeT and higher Fecarb/FeT and Fepy/FeT in the black shales of the Gyabula Formation might reflect the dissolution of iron oxides, with later partial escape of ferrous iron from sediment–water interface, and/or formation of carbonate-associated iron and pyrite under dysoxic–anoxic conditions within the upper layers of the sediment and probably in the bottom waters (Canfield, 1989). The Feox/FeT of red beds (0.295 on average) makes up 80% of the difference of FeHR/FeT between the Gyabula and Chuangde formations, and is not only higher than in the Gyabula Formation (0.10), but even higher than in modern continental margin and deep sea

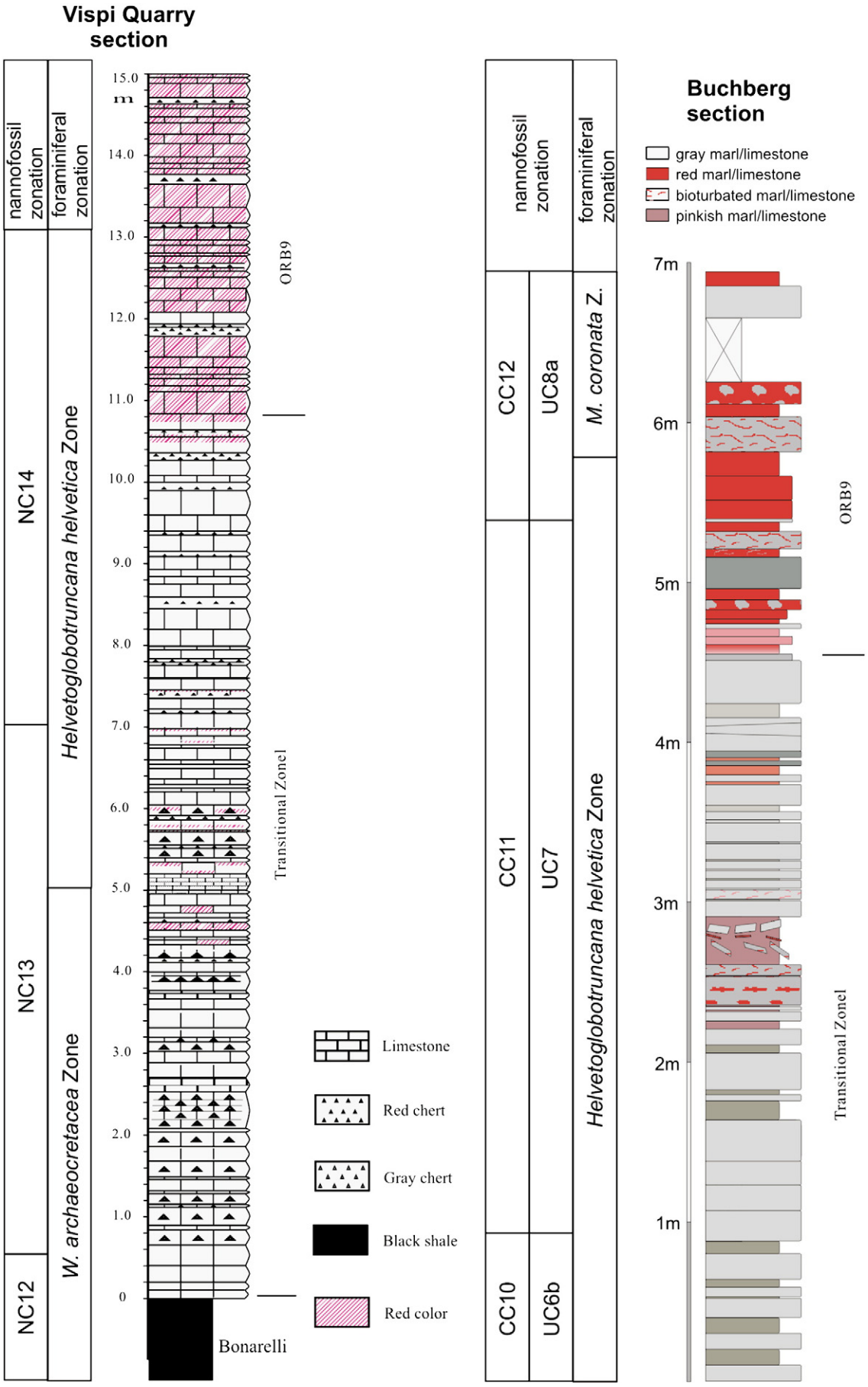

Fig. 5. Stratigraphic log of the OAE2–ORB9 transition in Vispi Quarry (revised from Hu et al., 2006a) and Bechberg section (from Neuhuber et al., 2007).

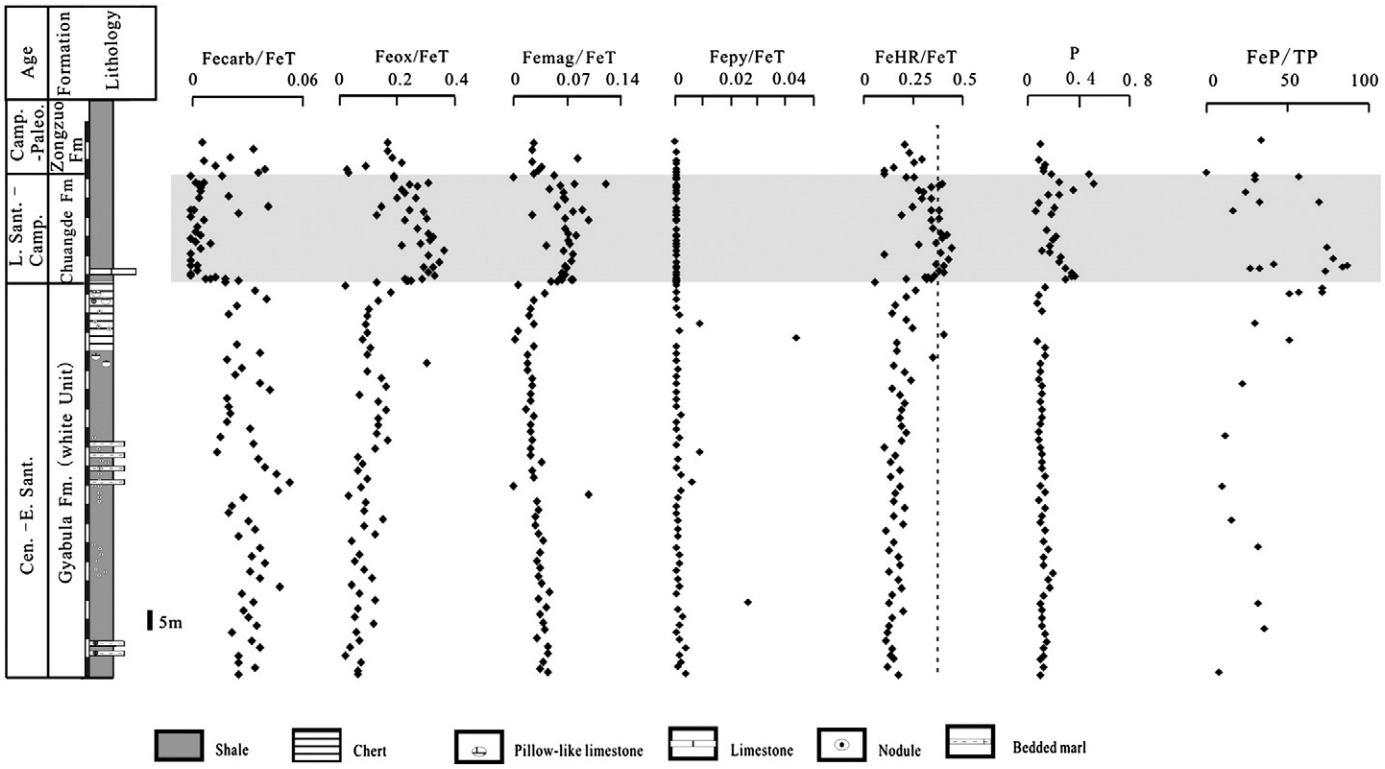

Fig. 6. Correlation and Variations of reactive iron burial records between black shales and CORBs and phosphorus (P), carbon isotope and Ba/Al in Chuangde section, South Tibet. Fecarb, Feox, Femag, Fepy and FeHR are carbonate-associated iron, ferric iron-oxides (goethite and hematite), magnetite, pyrite and total reactive iron (the sum of Fecarb, Feox, Femag, Fepy) respectively. Shaded area is the red beds of the Chuangde formation.

sediments (0.28 and 0.25, respectively) (Poulton and Raiswell, 2002). It is also higher than in the Jurassic and Cretaceous non-red normal marine sediments (0.16) in Western Europe (Poulton and Raiswell, 2002). This suggests that the ferric iron oxides in the red Chuangde Formation most probably formed during the syn-depositional to early diagenesis stage, similar to that in coeval CORBs in Italy (Channel et al., 1982) and Turkey (Eren and Kadir, 2001). Oxygen is the most abundant oxidant in the ocean (Froelich et al., 1979), and presence of iron oxides in pelagic red beds is an indicator that they formed in a highly oxic environment. The investigation of CORBs from the Eastern Alps, Austria also supports the hypothesis of highly oxic conditions for CORBs deposition (Neuhuber et al., 2007). Due to the close relation between the iron and phosphorus cycles, we also analyzed the total phosphorus in the black shales and red beds. Total phosphorus is higher in the Chuangde Formation (Fig. 6); which may be due to a greater amount of phosphorus being absorbed onto the iron oxides in the red beds (Slomp et al., 1996).

The organic carbon level in Chuangde Formation is extremely low, about 0.01–0.14% or even below the detection limit (Wang et al., 2005). In the black shale of Gyabula Formation, the organic carbon content averages about 0.5% (Wang et al., 2005). Low organic carbon content is a common feature of CORBs everywhere, being 0.3%, 0.07–0.17% and 0–0.005% in red beds from North Atlantic, Italy and Exmouth Plateau of Australia (Wang et al., 2009). Positive $\delta^{13}C_{carb}$ and $\delta^{13}C_{org}$ excursions occur in the mid-Cretaceous black shales (Wang et al., 2001), while negative $\delta^{13}C_{carb}$ and $\delta^{13}C_{org}$ excursions take place in the Upper Cretaceous red-beds, coincident with lower fractions of biogenic barite (Wang et al., 2005; Zou et al., 2005). These differences point to lower primary productivity in the ocean and less burial of organic matter when Chuangde Formation was deposited. Paleontological data from western Tethys also suggest a decrease of paleoproductivity in the ocean when the red beds were deposited (Kuhnt and Holbourn, 2005).

5. CORBs as a possible consequence of OAEs

Based on data reviewed above, here we propose the hypothesis that deposition of the Cretaceous oceanic red beds was a possible consequence of the Cretaceous oceanic anoxic events (Fig. 7). Enhanced amounts of organic carbon and pyrite burial during the Cretaceous OAEs (especially globally distributed OAE1a and OAE2) as indicated by sharp increases in $^{13}C/^{12}C$ isotope ratio in marine carbonate organic matter would have resulted in a large and abrupt fall in atmospheric CO_2 concentration (Arthur et al., 1988). For example, the OAE2 would have deposited about 1.6×10^{18} moles of organic carbon within 0.5 myr (Arthur et al., 1988). This led to a profound decrease (26% to 40–80%) in atmospheric pCO_2 (Kuypers et al., 1999; Barclay et al., 2010), enabling the appearance of plants using a CO_2-concentrating mechanism (C_4-type), which is illustrated by a North African plant community (Kuypers et al., 1999). The decrease in ρCO_2 probably induced significant global climatic cooling. But, it is still unknown that for how long the enhanced burial of organic carbon will result in decrease in ρCO_2 and global climatic cooling. Recently, a remarkable large cooling (5–11 °C) was discovered within the OAE2 interval which was interpreted to be response to the associated ρCO_2 drop (Sinninghe Damsté et al., 2010). They argued that the response of ρCO_2 drop and climatic cooling to enhanced burial of organic carbon during OAEs are probably concurrent and relatively short in time. Another view focused on the relative long time interval after the OAEs. For examples, the Late Aptian after the Early Aptian OAE1a and the latest Cenomanian OAE2 are in fact considered to be two cold snaps during the greenhouse Cretaceous. Direct evidence for Late Aptian global cooling is indicated by occurrences of glendonites and ice-rafted debris in the Canadian Sverdrup Basin, the West Svalbard Basin (Kemper, 1987) and in southeast Australia (Frakes et al., 1995). Isotopic evidence for a cool Late Aptian includes data from south temperate belemnites (Pirrie et al., 1995), glendonites (De Lurio and Frakes, 1999) and carbon isotopes (Weissert and Lini, 1991). Recently, Late Aptian global cooling was

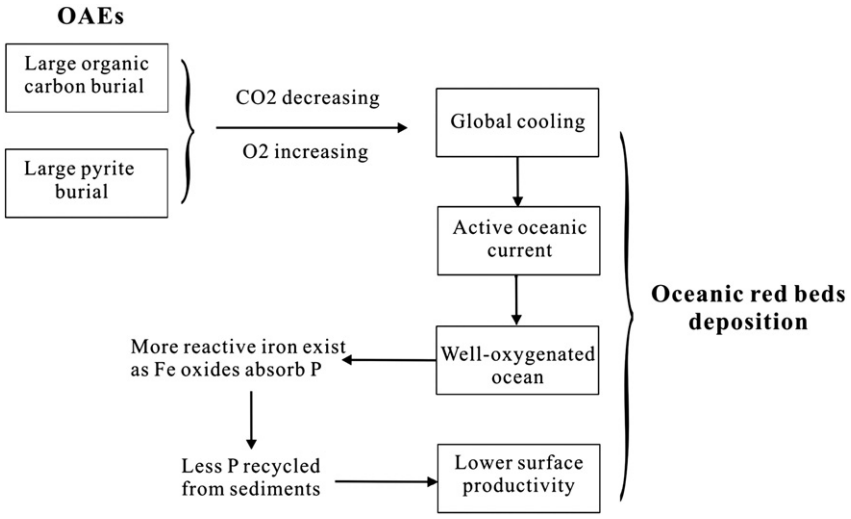

Fig. 7. Simplified hypothesis model for the transition from Cretaceous OAEs to CORBs.

suggested by a decline of Tethyan taxa of calcareous nannofossil assemblages and a subsequent biogeographic expansion of species of high latitudinal affinities (Mutterlose et al., 2009). Another "cool" period during the Cretaceous is the middle to late Turonian, with evidence from a positive oxygen isotopic excursion in marine limestones (Voigt and Wiese, 2000), brachiopods (Voigt et al., 2004) and foraminifers (Bornemann et al., 2008), an incursion of boreal faunas (ammonites, echinoids and inoceramids) into lower latitudes (Wiese and Voigt, 2002), data from organic geochemical proxy (TEX86) (Forster et al., 2007), and an Upper Turonian sequence boundary on the eastern U.S. continental shelf and elsewhere that represents sea level fall of 25–30 m that may be related to glacio-eustasy (Miller et al., 2003). Moreover, Bornemann et al. (2008) suggest that short periods of glaciation may have existed during middle Turonian, with ice sheets of about half the size of the modern Antarctic ice cap. We also note that one of the possible mechanisms for global cooling after the OAEs would be the general reduction in seafloor volcanic activity (Larson, 1991).

Global cooling would have enhanced formation of cold deep water, increasing its oxidizing capacity due to the greater content of dissolved oxygen. Furthermore, enhanced organic carbon burial during the Cretaceous OAEs would result in an equal addition of O_2 to the atmospheric oxygen reservoir, assuming a CO_2-to-O_2 photosynthetic ratio of 1:1 (Arthur et al., 1988, p.716). This would also have increased the oxidation potential of oceanic deep water. Therefore, an increase in pO_2 and global climate cooling with increased cold deep water formation resulting from organic carbon burial during the OAEs would have increased the oxidizing capacity of oceanic deep water and promoted formation of oceanic red beds. As we stated above, the transition from OAE1a to ORB1 during the Aptian took a relatively short time of 0.95–1.2 myr in western Tethys (Italy), and 2.9 myr in middle Tethys (Turkey). The transition from OAE2 to ORB9 took about 1.1 myr in western Tethys (Italy and Austria), but required a long time (> 9 myr) in Eastern Tethys (south Tibet). This model provides an effective mechanistic explanation for the development of CORBs, but it remains speculative pending further data collection.

During Late Cretaceous, especially Late Santonian–Campanian, the dissolved oxygen values remained relatively high as indicated by study of morphologic characteristics of benthic foraminifers in the global ocean (Kaiho, 1994). Besides well-oxygenated, cold deep water, several other processes may have contributed to the formation of CORBs. During the Late Santonian–Campanian when CORBs had a nearly worldwide distribution (Scott, 2009; Wang et al., 2009) (Fig. 1), bio-available phosphorus was at a low level (Föllmi, 1996). If bio-available phosphorus can be considered a first-order approximation of the total reactive phosphorus in the ocean (Föllmi, 1996), then the phosphorus reservoir in the Late Cretaceous was much lower than in the mid-Cretaceous, resulting in lower productivity. At the same time, the negative trend of the carbon isotope curve from pelagic carbonates is consistent with a global negative excursion (Jarvis et al., 2002). This is in contrast to the positive carbon isotope excursion associated with the mid-Cretaceous black shales (Leckie et al., 2002; Erba, 2004). Most of the organic carbon exported from the photic zone to the deeper waters was oxidized and only a small amount was buried. Geochemical modeling (Hanson and Wallmann, 2003) has shown that the organic carbon burial rate decreased during the latest Santonian to middle Campanian from an already low Turonian–early Santonian level, to a minimum at about 80 Ma. This shift is consistent with the significant global increase in inorganic/organic-carbon burial ratios of $68\times10^{18}/16\times10^{18}$ kg yr^{-1} (4.25:1) in the Early Cretaceous to $133\times10^{18}/20\times10^{18}$ kg yr^{-1} (6.65/1) in the Late Cretaceous (Budyko et al., 1987).

The oxic, lower productivity ocean can be further explained by the global climatic–oceanic change that occurred during the Late Cretaceous time. With global cooling (Huber et al., 2002) from a "hot-" to a "cool-" greenhouse climate during Turonian to Campanian (Clarke and Jenkyns, 1999), the equator-to-pole temperature gradient increased, progressively favoring the formation of large volumes of deep water at high-latitudes, particularly along the Antarctic margin (Otto-Bliesner et al., 2002), and increasing the turnover rates of the ocean. The largest drop in the global temperature occurred in early Campanian, with the change from "hot" to "cool" greenhouse climate (Clarke and Jenkyns, 1999; Huber et al., 2002), which may have led to increased oceanic turnover and therefore a well-ventilated deep ocean. Opening of the deep connection between the North and South Atlantic Oceans in the Campanian allowed deep waters generated in the southern hemisphere to circulate throughout the Atlantic basins (Poulsen et al., 2001). Furthermore, widening and deepening of the passages between Antarctica, Africa, and India, and between India and Australia allowed deep waters generated along the Antarctic margin to enter the Eastern Tethys and Panthalassic Oceans. The cooler high latitude deep waters introduced more oxygen to the deep ocean, so that more organic matter was oxidized, and iron oxides formed at the sediment–seawater interface. More phosphorus was adsorbed onto the iron-oxides and buried, slowing the regeneration of phosphorus from the sediments to the seawater (Colman and Holland, 2000). At the same time, continental input of phosphorus to the ocean decreased as result of cooler climate (Föllmi, 1996). The decrease of phosphorus cycling from the land to the ocean combined with the

reduced inventory of reactive phosphorus forced lower productivity in the ocean (Tyrrell, 1999).

The greenhouse climate of the mid-Cretaceous was likely related to major global volcanism and associated outgassing of CO_2. OAEs may be recognized as a negative feedback in response to sudden warming episodes preventing further acceleration of warming through removing the organic carbon from the ocean–atmosphere (CO_2), via increased productivity cycle, with organic carbon being buried in the deep ocean. However, the presence of oxic sediments (CORBs) within transition zones between individual OAEs indicate development of longer cooling-climate periods, therefore sharp swings in mid-Cretaceous climate, not considered by Cretaceous climate modelers. Such climate oscillations predate a change to predominantly cooler (icehouse) climate after Turonian time. Other paleoceanographic changes simultaneously were occurring at southern hemisphere and may have played roles as important as the climate change.

Acknowledgements

We thank the fellows from IGCP 463/494/555, and particularly to co-leaders Lubomir Jansa from in Canada, and Massimo Sarti in Italy, for valuable help concerning Cretaceous oceanic red beds deposition. We thank Karl Föllmi of the University of Lausanne, Switzerland, for providing phosphorus accumulation data. Thanks Mr. Ma Chao and Dr. Xi Chen who prepared Figs. 1 and 2. This manuscript benefited from the constructive reviews by guest editor Prof. Brad Sageman and one anonymous reviewer. This work was financially supported by National Key Basic Research Program of China Grant 2006CB701400, 111 Project of China Grant B07011 and Chinese National Science Foundation Grant 40332020.

Appendix 1. Cretaceous OAE's distributions

Appendix 1A OAE1a distribution.
Appendix 1B OAE2 distribution worldwide.
Appendix 1C references.

Appendix 2. Geochemical data from southern Tibet

Appendix 2A Analytical results of reactive iron species for Gyabula and Chuangde formation, southern Tibet.

Appendix 2B Summarization of ratio between reactive iron species and total iron in Gyabula and Chuangde Formation, South Tibet.

Appendix 2C Total phosphorus from Gyabula to Chuangde Formation, S. Tibet.

References

Arthur, M.A., Sageman, B.B., 1994. Marine black shales: a review of depositional mechanisms and environments of ancient deposits. Annual Review of Earth Planetary Science 22, 499–552.
Arthur, M.A., Dean, W., Pratt, L.M., 1988. Geochemical and climatic effects of increased marine organic carbon burial at the Cenomanian/Turonian boundary. Nature 335, 714–717.
Barclay, R.S., McElwain, J.C., Sageman, B.B., 2010. Carbon sequestration activated by a volcanic CO_2 pulse during Ocean Anoxic Event 2. Nature Geoscience 3, 205–208.
Baudin, F., Fiet, N., Coccioni, R., Galeotti, S., 1998. Organic matter characterisation of the Selli Level (Umbria-Marche Basin, central Italy). Cretaceous Research 19, 701–714.
Berner, R.A., 2003. The long-term carbon cycle, fossil fuels and atmospheric composition. Nature 426, 323–326.
Berner, R.A., Kothavala, Z., 2001. GEOCARB III: a revised model of atmospheric CO_2 over Phanerozoic time. American Journal of Science 301, 182–204.
Bice, K.L., Norris, R.D., 2002. Possible atmospheric CO_2 extremes of Middle Cretaceous (late Albian–Turonian). Paleoceanography 17, 778–795.
Bornemann, A., Norris, R.D., Friedrich, O., Beckmann, B., Schouten, S., Sinninghe Damsté, J., Vogel, J., Hofmann, P., Wagner, T., 2008. Isotopic evidence for glaciation during the Cretaceous supergreenhouse. Science 319 (5860), 189–192.
Budyko, M.I., Ronov, A.B., Yanshin, A.L., 1987. History of the Earth's Atmosphere. Springer, Berlin.
Canfield, D.E., 1989. Reactive iron in marine sediments. Geochimica et Cosmochimica Acta 53, 619–632.
Channel, J.E.T., Freeman, R., Heller, F., Lowrie, W., 1982. Timing of diagenetic haematite growth in red pelagic limestones from Gubbio (Italy). Earth and Planetary Science Letters 58, 189–201.
Clarke, L.J., Jenkyns, H.C., 1999. New oxygen isotope evidence for long-term Cretaceous climatic change in the Southern Hemisphere. Geology 27, 699–702.
Coccioni, R., Nesci, O., Tramontana, M., Wezel, F.C., Moretti, E., 1987. Descrizione di un livello-guida 'radiolaritico-bituminoso-ittiolitoco' alla base delle Marne a Fucoidi nell'Appennino unbro-marchigiano. Bollettino. Societa Geologica Italiana 106, 183–192.
Coccioni, R., Nesci, O., Tramontana, M., Wezel, F.C., Battistini, F., Pallecchi, P., 1989. Stratigraphy and mineralogy of the Selli Level (Early Aptian) at the base of the Marne a Fucoidi in the Umbro-Marchean Apennines, Italy. In: Wiedmann, J. (Ed.), Cretaceous of the Western Tethys. : Proceedings 3rd International Cretaceous Symposium, Tübingen 1987. E. Schweizerbart'sche Verlagsbuchhandlung, Stuttgart, pp. 563–584.
Coccioni, R., Galeotti, S., Ragni, D., 1992. Litho- and biostratigraphy of the Scaglia Bianca Formation (Late Albian-Late Cenomanian) in the Umbria-Marche Apennines (Italy). 6th Annual Meeting of IGCP 262 (Tethyan Cretaceous Correlation), vol. 4. Cretaceous Facies in Orogenic Belts, Athens.
Colman, A.S., Holland, H.D., 2000. The global diagenetic flux of phosphorus from marine sediments to the oceans: redox sensitivity and the control of atmospheric oxygen levels. In: Glenn, C.R., Prévôt-Lucas, L., Lucas, J. (Eds.), Marine Authigenesis: From Global to Microbial SEPM, Special Publication, vol. 66, pp. 53–75.
De Lurio, J.L., Frakes, L.A., 1999. Glendonites as a paleoenvironmental tool: implications for early Cretaceous high latitude climates in Australia. Geochimica et Cosmochimica Acta 63, 1039–1048.
Erba, E., 1988. Aptian–Albian calcareous nannofossil biostratigraphy of the Scisti a Fucoidi cored at Piobbico (Central Italy). Rivista Italiana di Paleontologia e Stratigrafia 94, 249–284.
Erba, E., 2004. Calcareous nannofossils and Mesozoic oceanic events. Marine Micropaleontology 52, 85–106.
Eren, M., Kadir, S., 2001. Colour genesis of Upper Cretaceous pelagic red sediments within the Eastern Pontides, NE Turkey. Yerbilimleri 24, 71–79.
Föllmi, K.B., 1996. The phosphorus cycle, phosphogenesis and marine phosphate-rich deposits. Earth Science Reviews 40, 55–124.
Forster, A., Schouten, S., Baas, M., Damste, J.S.S., 2007. Mid-Cretaceous (Albian–Santonian) sea surface temperature record of the tropical Atlantic Ocean. Geology 35, 919–922.
Frakes, L.A., Francis, J.E., Syktus, J.I., 1992. Climate modes of the Phanerozoic. Cambridge University Press, Cambridge, United Kingdom.
Frakes, L., Alley, N., Deynoux, M., 1995. Early Cretaceous ice rafting and climate zonation in Australia. International Geology Review 37, 567–583.
Froelich, P.N., Klinkhammer, G.P., Bender, M.L., Luedtke, N.A., Heath, G.R., Cullen, D., Dauphin, P., Hammond, D., Hartman, B., Maynard, V., 1979. Early oxidation of organic matter in pelagic sediments of the eastern equatorial Atlantic: Suboxic diagenesis. Geochimica et Cosmochimica Acta 43, 1075–1090.
Glasby, G.P., 1991. Mineralogy, geochemistry, and origin of Pacific red clays: a review. New Zealand Journal of Geology and Geophysics 34, 167–176.
Hanson, K.W., Wallmann, K., 2003. Cretaceous and Cenozoic evolution of seawater composition, atmospheric O_2 and CO_2: a model perspective. American Journal of Science 303, 94–148.
Haq, B.U., Hardenbol, J., Vail, P.R., 1987. Chronology of fluctuating sea levels since the Triassic. Science 235, 1156–1167.
Hu, X.M., Jansa, L., Sarti, M., 2006a. Mid-Cretaceous oceanic red bed in the Umbria–Marche Basin, central Italy: Constraints on paleoceanography and paleoclimate. Palaeogeography, Palaeoclimatology, Palaeoecology 233, 163–186.
Hu, X.M., Wang, C.S., Jansa, L., 2006b. Upper Cretaceous oceanic red beds in southern Tibet: Lithofacies, environments, and colour origin. Science in China. Series D: Earth Sciences 36, 811–821.
Hu, X.M., Cheng, W.B., Ji, J.F., 2009. Origin of Cretaceous oceanic red beds from the Vispi Quarry section, central Italy: visible reflectance and inorganic geochemistry. In: Hu, X.M., Wang, C.S., Scott, R.W., Wagreich, M., Jansa, L. (Eds.), Cretaceous Oceanic Red Beds: Stratigraphy, Composition, Origins and Paleoceanographic and Paleoclimatic Significance: SEPM Special Publication, vol. 91, pp. 183–197.
Huber, B.T., Norris, R.D., MacLeod, K.G., 2002. Deep-sea paleo-temperature record of extreme warmth during the Cretaceous. Geology 30, 123–126.
Jarvis, I., Mabrouk, A., Moody, R.T.J., de Cambrera, S., 2002. Sea-level change and correlation of the Tethyan and Boreal realms. Palaeogeography, Palaeoclimatology, Palaeoecology 141, 1–12.
Kaiho, K., 1994. Planktonic and benthic foraminiferal extinction events during the last 100 m.y. Palaeogeography, Palaeoclimatology, Palaeoecology 111, 45–71.
Kemper, E., 1987. Das Klima der Kreide-Zeit. Geologisches Jahrbuch A 96, 5–185.
Kuhnt, K., Holbourn, A., 2005. Late Cretaceous deep-water benthic foraminiferal biofacies and lithofacies of western and eastern Tethys. Earth Science Frontier 26, 81–104 (in Chinese with English Abstracts).
Kuypers, M.M., Pancost, R.D., Damste, J.S., 1999. A large and abrupt fall in atmospheric CO_2 concentration during Cretaceous times. Nature 399, 342–345.
Larson, R.L., 1991. Geological consequences of superplumes. Geology 19, 963–966.
Leckie, R.M., Bralower, T.J., Cashman, R., 2002. Oceanic anoxic events and plankton evolution: Biotic response to tectonic forcing during the mid-Cretaceous. Paleoceanography 17, 623–642.
Lyons, T.W., Severman, S.A., 2006. Critical look at iron paleoredox proxies: new insights from modern euxinic marine basins. Geochemica et Cosmachimica Acta 70, 5698–5772.

Miller, K.G., Sugarman, P.J., Browning, J.V., Kominz, M.A., Hernández, J.C., Olsson, R.K., Wright, J.D., Feigenson, M.D., van Sickel, W., 2003. Late Cretaceous chronology of large, rapid sea-level changes: glacioeustasy during the greenhouse world. Geology 31, 585–588.

Mutterlose, J., Bornemann, A., Herrle, J., 2009. The Aptian–Albian cold snap: evidence for "mid" Cretaceous icehouse interludes. Neues Jahrbuch für Geologie und Paläontologie Abhandlungen 252, 217–225.

Neuhuber, S., Wagreich, M., Wendler, I., Spötl, C., 2007. Turonian Oceanic Red Beds in the Eastern Alps: concepts for palaeoceanographic changes in the Mediterranean Tethys. Palaeogeography, Palaeoclimatology, Palaeoecology 251, 222–238.

Otto-Bliesner, B.L., Brady, E.C., Shields, C., 2002. Late Cretaceous ocean: coupled simulations with National Center for Atmospheric Research Climate System Model. Journal of Geophysical Research 107 (NO.D2). doi:10.1029/2001DJ000821.

Pirrie, D., Doyle, P., Marshall, J.D., Ellis, G., 1995. Cool Cretaceous climates: new data from the Albian of Western Australia. Journal of the Geological Society 152, 739–742.

Poulsen, J.C., Barron, J.E., Arthur, A.M., Peterson, H.W., 2001. Response of the mid-Cretaceous global oceanic circulation to tectonic and CO_2 forcings. Paleoceanography 16, 1–17.

Poulton, S.W., Canfield, D.E., 2005. Development of a sequential extraction procedure for iron: implications for iron partitioning in continentally derived particulates. Chemical Geology 214, 209–221.

Poulton, S.W., Raiswell, R., 2002. The low-temperature geochemical cycle of iron: from continental fluxes to marine sediment deposition. American Journal of Sciences 302, 774–805.

Premoli Silva, I., Sliter, V.W., 1994. Cretaceous planktonic foraminiferal biostratigraphy and evolutionary trends from the Bottaccione section, Gubbio (Italy). Paleontographia Italica 82, 1–89.

Raiswell, R., Canfield, D.E., 1998. Sources of iron for pyrite formation in marine sediments. American Journal of Sciences 298, 219–245.

Ruddiman, W.F., 2001. Earth's Climate, Past and Future. W.H. Freeman, New York.

Schlanger, S.O., Jenkyns, H.C., 1976. Cretaceous oceanic anoxic events: causes and consequences. Geologie en Mijnbouw 55, 179–184.

Scott, R.W., 2009. Chronostratigraphic database for Upper Cretaceous Oceanic Red Beds (CORBS). In: Hu, X.M., Wang, C.S., Scott, R.W., Wagreich, M., Jansa, L. (Eds.), Cretaceous Oceanic Red Beds: Stratigraphy, Composition, Origins and Paleoceanographic and Paleoclimatic Significance: SEPM Special Publication, 91, pp. 35–57.

Sinninghe Damsté, J.S., van Bentum, E.C., Reichart, G.-J., Pross, J., Schouten, S., 2010. A CO_2 decrease-driven cooling and increased latitudinal temperature gradient during the mid-Cretaceous Oceanic Anoxic Event 2. Earth and Planetary Science Letters 293 (1–2), 97–103.

Slomp, C.P., Van der Gaast, S.J., Van Raaphorst, W., 1996. Phosphorus binding by poorly crystalline iron oxides in North Sea sediments. Marine Chemistry 52, 55–73.

Takashima, R., Kawabe, F., Nishi, H., Moriya, K., Wani, R., Ando, H., 2004. Geology and stratigraphy of forearc basin sediments in Hokkaido, Japan: cretaceous environmental events on the Northwest Pacific margin. Cretaceous Research 25, 365–390.

Tarduno, J.A., Brinkman, D.B., Renne, P.R., Cottrell, R.D., Scher, H., Castillo, P., 1998. Evidence for extreme climatic warmth from Late Cretaceous Arctic vertebrates. Science 282, 2241–2243.

Tornaghi, M.E., Premoli Silva, I., Ripepe, M., 1989. Lithostratigraphy and planktonic foraminiferal biostratigraphy of the Aptian–Albian "Scisti a Fucoidi" in the Piobbico core, Marche, Italy: background for cyclostratigraphy. Rivista Italiana di Paleontologia e Stratigrafia 95, 223–264.

Tyrrell, T., 1999. The relative influence of nitrogen and phosphorus on oceanic primary production. Nature 400, 525–529.

Voigt, S., Wiese, F., 2000. Evidence for Late Cretaceous (Late Turonian) climate cooling from oxygen–isotope variations and palaeobiogeographic changes in Western and Central Europe. Journal of the Geological Society 157, 737–743.

Voigt, S., Gale, A.S., Fl gel, S., 2004. Midlatitude shelf seas in the Cenomanian–Turonian greenhouse world: temperature evolution and North Atlantic circulation. Paleoceanography 19. doi:10.1029/2004PA001015.

Wagreich, M., Neuhuber, S., Egger, J., Wendler, I., Scott, R.W., Malata, E., Sanders, D., 2009. Stratigraphy and facies of Cretaceous oceanic red beds (CORBs) in the Eastern Alps (Austria): pelagic passive margin vs. active margin depositional settings. In: Hu, X.M., Wang, C.S., Scott, R.W., Wagreich, M., Jansa, L. (Eds.), Cretaceous Oceanic Red Beds: Stratigraphy, Composition, Origins and Paleoceanographic and Paleoclimatic Significance: SEPM Special Publication, 91, pp. 73–88.

Wan, X.Q., Wignall, P.B., Zhao, W.J., 2003. The Cenomanian–Turonian extinction and oceanic anoxic event: evidence from South Tibet. Palaeogeography, Palaeoclimatology, Palaeoecology 199, 283–298.

Wan, X.Q., Lamolda, M.A., Si, J.L., Li, G.B., 2005. Foraminiferal stratigraphy of Late Cretaceous red beds in southern Tibet. Cretaceous Research 26, 43–48.

Wang, C.S., Hu, X.M., Jansa, L.F., Wan, X.Q., Tao, R., 2001. The Cenomanian–Turonian oceanic anoxic event in southern Tibet. Cretaceous Research 22, 481–490.

Wang, C.S., Hu, X.M., Jansa, L., Sarti, M., Scott, W.R., Li, X.H., 2005. Upper Cretaceous oceanic red beds in southern Tibet: a major change from anoxic to oxic condition. Cretaceous Research 26, 21–32.

Wang, C.S., Hu, X.M., Huang, Y.J., Scott, R.W., Wagreich, M., 2009. Overview of Cretaceous Oceanic Red Beds (CORBs): a window on global oceanic and climate change. In: Hu, X.M., Wang, C.S., Scott, R.W., Wagreich, M., Jansa, L. (Eds.), Cretaceous Oceanic Red Beds: Stratigraphy, Composition, Origins and Paleoceanographic and Paleoclimatic Significance: SEPM Special Publication, 91, pp. 13–33.

Weissert, H., Lini, A., 1991. Ice age interludes during the time of Cretaceous greenhouse climate? In: Müller, D.W., McKenzie Weissert, J.A., H. (Eds.), Controversies in Modern Geology. Academy Press, London, pp. 171–191.

Wendler, I., Wendler, J., Neuhuber, S., Wagreich, M., 2009. Productivity fluctuations and orbital cyclicity during onset of Early to Middle Turonian marine red bed formation (Austrian Eastern Alps). In: Hu, X.M., Wang, C.S., Scott, R.W., Wagreich, M., Jansa, L. (Eds.), Cretaceous Oceanic Red Beds: Stratigraphy, Composition, Origins and Paleoceanographic and Paleoclimatic Significance: SEPM Special Publication, vol. 91, pp. 13–33.

Wiese, F., Voigt, S., 2002. Late Turonian (Cretaceous) climate cooling in Europe: faunal response and possible causes. Geobios 35, 65–77.

Yilmaz, I.O., 2008. Cretaceous pelagic red beds and black shales (Aptian–Santonian), NW Turkey: global oceanic anoxic and oxic events. Turkish Journal of Earth Sciences 17, 263–296.

Zou, Y.R., Kong, F., Peng, P.A., Hu, X.M., Wang, C., 2005. Organic geochemical characterization of Upper Cretaceous oxic oceanic sediments in Tibet, China: a preliminary study. Cretaceous Research 26, 65–71.